Composites Science and Technology 199 (2020) 108367

Contents lists available at ScienceDirect

Composites Science and Technology

journal homepage: http://www.elsevier.com/locate/compscitech

Laser induced graphene in fiberglass-reinforced composites for strain and damage sensing

LoriAnne Groo [a], Jalal Nasser [a], Lisha Zhang [b], Kelsey Steinke [c], Daniel Inman [a], Henry Sodano [a,b,c,*]

[a] Department of Aerospace Engineering, University of Michigan, Ann Arbor, MI, 48109, United States
[b] Department of Macromolecular Science and Engineering, University of Michigan, Ann Arbor, MI, 48109, United States
[c] Department of Materials Science and Engineering, University of Michigan, Ann Arbor, MI, 48109, United States

ARTICLE INFO

Keywords:
Fiberglass-reinforced composites
Laser induced graphene
Piezoresistive sensing
Structural health monitoring
Multifunctional composites

ABSTRACT

Structural health monitoring of fiber-reinforced composite materials is of critical importance due to their use in challenging structural applications where low density is required and the designs typically use a low factor of safety. In order to reduce the need for external sensors to monitor composite structures, recent attention has turned to multifunctional materials with integrated sensing capabilities. This work use laser induced graphene (LIG) to create multifunctional structure with embedded piezoresistivity for the simultaneous and in-situ monitoring of both strain and damage in fiberglass-reinforced composites. The LIG layers are integrated during the fabrication process through transfer printing to the surface of the prepreg before being laid up into the ply stack, and are thus located in the interlaminar region of the fiberglass-reinforced composite. The methods used in this work are simple and require no treatment or modification to the commercial fiberglass prepreg prior to LIG transfer printing which is promising for industrial scale use. The performance of the piezoresistive interlayer in monitoring both strain and damage in-situ are demonstrated via three-point bend and tensile testing. Additionally, the interlaminar properties of the fiberglass composites were observed to be largely maintained with the LIG present in the interlaminar region of the composite, while the damping properties were found to be improved. This work therefore introduces a novel multifunctional material with high damping and fully integrated sensing capabilities through a cost-effective and scalable process.

1. Introduction

Fiberglass-reinforced composites exhibit high strength and stiffness in addition to excellent fatigue resistance which have made them increasingly common in multiple fields including the aerospace, marine, aeronautics, and automobile industries [1]. However, damage in composite materials is difficult to detect and often not visible, which, combined with the importance of these structural applications, increases the need for monitoring damage and state change via structural health monitoring (SHM). The ability to continually assess the condition of composite materials without requiring their removal from service both reduces maintenance costs and improves the safety of the structure. Fiberglass-reinforced composites are well-suited for extreme loading conditions due to their high specific strength, however, the complex nature of the loading conditions combined with the laminar nature of composite materials makes them prone to damage due to inter-ply delamination, brittle fiber breakage, and microdamage within the polymer matrix. Multiple methods have been investigated over the past several years to detect these types of damage including X-ray computed microtomography (micro-CT) [2,3], acoustic emission testing (AET) [4–6], fiber optics [7,8], and resistance-based strain and damage sensing [9,10]. Of these methods, resistance-based sensing using embedded conductors has received significant research interest for several reasons including: the simplicity of the methodology, the elimination of the need for external sensors or bulky embedded sensing materials, and the in-situ monitoring of both strain and damage simultaneously.

Initially, resistance-based damage and strain sensing was employed with only conductive carbon fiber reinforcement, as it was intended to take advantage of the inherent piezoresistivity of the fiber. Piezoresistivity is a material property that defines its ability to change resistance with respect to the strain. The piezoresistivity of carbon fiber enables their composites to show a change in impedance corresponding

* Corresponding author. Department of Aerospace Engineering, University of Michigan, Ann Arbor, MI, 48109, United States.
E-mail address: hsodano@umich.edu (H. Sodano).

https://doi.org/10.1016/j.compscitech.2020.108367
Received 16 March 2020; Received in revised form 15 June 2020; Accepted 16 July 2020
Available online 25 July 2020

to a change in strain which can be tracked through a simple in-situ resistance measurement [11,12]. Using the common four-probe measurement technique, current is applied through the loaded specimen and the corresponding voltage is measured, allowing for the calculation of the resistance using Ohm's law. Furthermore, as damage occurs in the form of fiber fracture, a sudden increase in the electrical impedance of the composite samples can be observed due to the sudden breaking of conductive pathways. This methodology has been utilized to detect various forms of damage in carbon fiber-reinforced composites including fiber fracture in tensile loading, impact damage, and flexural strain [11–17]. However, this approach requires electrically conductive fiber reinforcement and is thus limited in its application across the various forms of composite materials.

Since the initial research on polymer matrix composites with conductive carbon fiber reinforcement, resistance-based sensing has since been expanded to include insulating fibers, such as glass [18], through the addition of conductive carbon-based nanofillers. These nanofillers include, but are not limited to, carbon black, graphene oxide, and carbon nanotubes (CNTs) [9,18–21]. For example, graphene oxide coated E-glass fibers were shown to be capable of in-situ tensile strain sensing via electrical resistance measurements, while also displaying improved interlaminar shear strength, flexural modulus, and flexural strength when compared to neat fibers [20]. Additionally, CNTs have gained interest due to their multifunctional benefits; when used in reinforced fiberglass composites they were shown to increase the interfacial shear strength and improved fatigue life in addition to endowing piezoresistivity to the fiberglass composites [22,23]. Gao et al. demonstrated the utility of the piezoresistivity by dispersing CNTs throughout the epoxy matrix and making in-situ measurements of impact damage [24]. Multiple other efforts have also studied the effective use of CNTs dispersed in the matrix of fiberglass composites to track fatigue loading via electrical impedance measurements [25,26]. However, the integration of CNTs within the matrix of fiber-reinforced composites has been shown to pose issues due to their tendencies to form agglomerations, which limits the formation of percolating networks of the conductive filler leading to reduced piezoresistive sensing [27,28]. To avoid dispersing CNTs in the matrix, Alexopoulos et al. demonstrated the usefulness of CNTs in the form of a CNT fiber for tracking both tensile and flexural loading and damage in fiberglass composites [29]. The CNT fiber was embedded in the composite during the fabrication process, however the sensing area was limited to the physical location of the fiber as the sensing material was not fully distributed throughout the composite. Although CNTs have been shown to be effective in detecting damage and sensing strain, the methods used to include them within composites are complex, expensive, and require considerable pre-processing which limits the scale-up potential for implementation of the self-sensing materials.

Recently, Lin et al. demonstrated the ability to form graphene nanostructures on polymer surfaces using a commercial CO_2 infrared laser [30]. The resulting graphene layers are porous and tailorable as well as being highly conductive and piezoresistive. Since the discovery of laser induced graphene (LIG), the potential applications for this material have rapidly grown to include micro-supercapacitors [31,32], biomedical sound sensing [33], and strain sensing [34], among others [34–38]. Investigating the use of the LIG for piezoresistive sensing, Rahimi et al. utilized the LIG to form a highly flexible strain sensor fabricated by transferring LIG printed onto Kapton® to polydimethylsiloxane polymer (PDMS) [39]. The flexible PDMS was then attached to a common glove which was used to track the motion of a finger and hand. Additionally, Wang et al. explored the sensing capability of the LIG by fabricating a standalone buckypaper comprised entirely of LIG [40]. The buckypaper was then included in a prepreg fiber-reinforced composite and the resistance was shown to increase with increasing stress and strain, however, the structural effects of the buckypaper on the host composite were not investigated. Although the strain sensing capabilities of LIG are beginning to be explored, no research to this point has utilized this novel sensing interface to track both strain and damage of commercial fiberglass prepreg composite during flexural and tensile loading. Nonetheless, the simplicity of this methodology makes it ideally suited for large-scale production and application in fiber-reinforced composites.

This research uses the simple LIG methodology to print fuzzy graphene layers directly onto commercial polyimide tape using a common CO_2 infrared laser. Once the graphene coating is complete, it is simply transfer printed onto the surface of commercial unidirectional fiberglass prepreg. Multiple layers of prepreg with LIG are then combined using traditional layup methods, resulting in the full integration of the LIG sensing component within the interlaminar regions of the fiberglass-reinforced polymer matrix composite. The composite plates are then cut into samples for dynamic mechanical analysis to examine the viscoelastic properties of the material, mechanical testing via short beam shear testing to evaluate the short beam strength, and both three-point bend and tensile testing to investigate the sensing capabilities of the material. Therefore, both the structural and sensing capabilities of the LIG interlayer are considered for large-scale application as a multifunctional structural material. This work notably uses processes which are more scalable than current alternatives, and the outcome is a fully integrated sensing component within a structural composite, thus removing any need for the bonding of external sensors.

2. Material and methods

2.1. LIG and composite fabrication

The LIG interlayer used in this research was fabricated based on the work of Lin et al. [30], however, the transfer printing process has not yet been developed or used with LIG and fiberglass prepreg. To generate the LIG, an Epilog Zing 16 universal laser system with a 40 W CO_2 infrared laser was used to generate the textured graphene film on 2 mil (0.0254 mm) thick Kapton® polyimide tape sheets at a pulsing density of 400 dots per inch (DPI) and power of 14%, as illustrated in Fig. 1a. During the laser irradiation, the polyimide film is used as a precursor for the LIG which is generated by a pulsed laser that photothermally converts the sp^3-carbon atoms to sp^2-carbon atoms without the need for an external graphene source [30]. Once the LIG layer was complete, the graphene was transferred to a fiberglass prepreg (CYCOM® E773 epoxy prepreg with S-2 glass fiber reinforced roving) using a constant-pressure rolling process, where the prepreg was slightly heated to approximately 80 °C in order to ensure the matrix was softened for the embedment of the LIG (Fig. 1b). During this process, the LIG coating is rolled onto the tacky prepreg causing the LIG to adhere to the prepreg surface and detach from the remaining polyimide film. As a result, the LIG was completely transferred from the Kapton® tape to the tacky surface of the prepreg, yielding a conductive surface covering the entire plane of the fiberglass prepreg. Following the introduction of the LIG, four sets of samples were fabricated for both mechanical and functional analysis as shown in Fig. 1c. First, 16 layers of unidirectional LIG coated fiberglass were combined to assess the short beam shear properties. To evaluate the damping characteristics, 3 layers of unidirectional LIG coated fiberglass were combined, while 3 layers of fiberglass with LIG were also stacked together at [+45/-45/+45]° for three-point bend testing. Finally, two sets of 3-ply composites of unidirectional and [+45/-45/+45]° plies were fabricated for tensile testing to assess the ability of both unidirectional and angled composites to detect tensile strain. Neat fiberglass samples were also fabricated using the same number of layers for both the short beam shear and dynamic testing to provide a basis for comparison. The prepreg layers for each composite layup were then pressed at 127 °C and 100 psi (689.5 kPa) in a hot press under vacuum for 2 h as is recommended by the manufacturer. Once the composite layups were completed, the samples were cut to their respective widths and lengths as recommended by each ASTM standard, however additional length was added to the three-point bend samples for the addition of wire leads

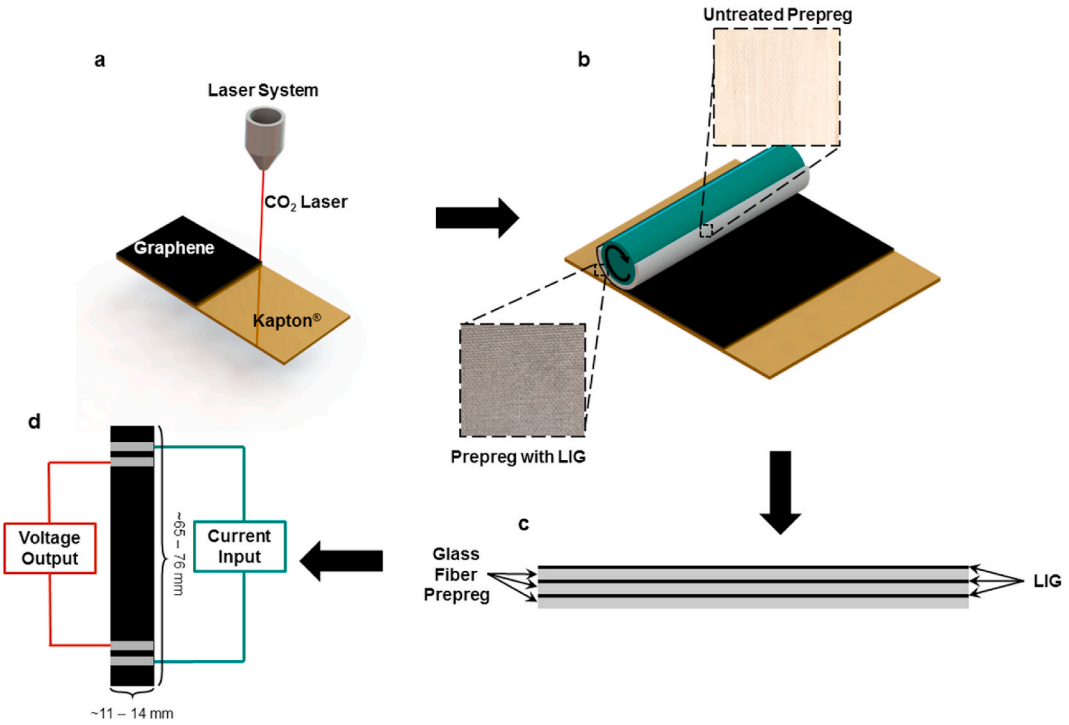

Fig. 1. (a) Schematic of LIG process on polyimide tape. (b) Schematic of LIG transfer process. (c) Schematic of composite layup. (d) Schematic of completed test specimen.

used for the application of current and voltage measurements during testing. Additionally, to reduce slipping and create a non-conductive barrier between the sample and the load frame, woven fiberglass composite tabs were added to the ends of the tensile samples using high shear strength epoxy (Loctite® 9430™ Hysol®). Finally, four silver paint rings were added to each three-point bend and tensile sample with two rings at each end as can be seen in Fig. 1d. Since the LIG was located throughout the entire plane of the fabricated composite, the silver paint around the edges formed a conductive contact between plies. The outer rings served as contact points where the current was applied, and the inner rings were contacts for voltage measurements using the four-probe method for resistance monitoring. Wire leads (33-gauge copper wire) were then added to each silver paint ring using a combination of silver paint and epoxy.

2.2. Mechanical testing

After the inclusion of the LIG in the fiberglass-reinforced composites, short beam specimens were cut from the 3 mm thick panel to dimensions of 6 mm wide by 18 mm long, as specified in ASTM standard D2344. Three-point bend testing was then performed to assess the short beam strength of the composites containing LIG compared to neat fiberglass prepreg samples. The primary mode of failure in short beam shear testing is located within the interlaminar region, thus this method of testing provides crucial information regarding the effect of the LIG on the inter-ply strength of the composite. The tests were completed per ASTM standard D2344 with a span to thickness ratio of 4:1, and 12 samples were tested for each data set using an Instron load frame (Model 5982) with 100 kN load cell. The thickness of both the neat fiberglass composite and the LIG coated fiberglass composite was approximately 3 mm, thus the addition of the LIG interlayer was not found to increase the thickness of the composite samples. The sample thickness has a significant effect on the short beam shear strength [41], therefore, since changes in the thickness were negligible, a direct comparison between the neat samples and samples containing LIG was possible.

To evaluate the viscoelastic properties of the fiberglass-reinforced composites containing LIG, dynamic mechanical analysis was performed on 3 neat fiberglass samples and 3 fiberglass samples containing LIG. The composite samples, which were approximately 0.8 mm in thickness, were cut to dimensions of 60 mm in length and 10 mm in width in accordance with the suggested testing parameters for the TA Instruments Q800 dynamic mechanical analyzer (DMA). The composite beams were then tested using a dual cantilever clamp at 10 Hz from room temperature (~20–25 °C) to 200 °C with heating at a ramp rate of 5 °C/min. Neat fiberglass-reinforced composites without LIG were also tested using the same setup and testing parameters for direct comparison of the viscoelastic properties of the composites. To evaluate the relative damping of the composites, the ratio between the loss modulus (E″) and storage modulus (E′), known as tan δ, was measured directly by the DMA and was the primary parameter considered here. Furthermore, to confirm that the addition of the LIG does not significantly affect the curing process of the LIG, two samples, one neat fiberglass prepreg and one fiberglass prepreg with LIG were tested using differential scanning calorimetry analysis (DSC). The samples were heated to 126.67 °C at a rate of 2.75 °C/min, following the curing cycle recommended by the manufacturer, and the heat flow was monitored to evaluate the cure.

2.3. Tensile testing

The cured LIG coated composites were tested through tensile testing according to ASTM standard D3039 to evaluate the ability of the LIG surfaces to sense tensile strain. Both the unidirectional and ±45° composite samples were cut to dimensions specified by ASTM standard D3039 for tensile testing with a gauge length of ~75 mm. An Instron model 5982 with a 100 kN load cell was again used to load the sample and measure the applied load. For the application of the four-probe resistance measurement, 3 mA of current was applied through the sample using the two outermost silver paint rings, and the corresponding voltage was measured between the two innermost silver paint rings using a NI 4431 data acquisition system (DAQ) (Fig. 1d). The resistance of the sample for the duration of the test was calculated using Ohm's law after the completion of the test. For clearer visualization and detection of

sudden increases in impedance, the second derivative of the percent change in impedance was calculated numerically by taking the numerical gradient of the response with respect to time. To confirm the occurrence of damage through acoustic emissions, a high frequency microphone (PCB 426A05) was attached to the test frame close to the sample and was read through a PCB 482A16 signal conditioner which was then connected to the same NI 4431 DAQ. For reference, four unidirectional and four angle ply samples were tested. In addition to monotonic tensile tests, quasi-static cyclic loading tests were performed at approximately 50% of the maximum stress on four additional samples. This was completed for greater assessment of the ability of the LIG on the fiberglass to repeatedly track low levels of strain prior to fiber breakage or delamination within the composite specimen. One pre-cycle of loading and unloading was used to allow the response to stabilize prior to data collection. To more accurately detect small changes in resistance, the sample was connected to a Wheatstone bridge for which the input voltage was provided by a DC power supply (Hewlett Packard model 6217A), and the response of which was read through a millivolt amplifier (Omega TM model MN1400-4). For greater strain monitoring accuracy at such low load values, a VISHAY® micro-measurements & SR-4 general purpose strain gauge (350 ± 0.2% Ω, 2.00 gauge factor) mounted to the sample surface was used in combination with a Wheatstone bridge and a Transducer Techniques model TMO-2 signal conditioner.

2.4. Three-point bend

To characterize the ability of the LIG coated fiberglass samples to detect flexural strain and the resulting damage, ASTM standard D7264 three-point bend testing was performed on eight total samples. An angle ply composite (3 plies) was cut to beams of dimensions ~13 mm wide by ~76 mm long as specified by ASTM standard D7264 for three-point bend. The Instron load frame (model 5982) and 100 kN load cell were again used, and Kapton® tape was added to the contact points between the LIG coated composite sample and the load frame to eliminate electrical interference. To subject the sample to high levels of flexural strain and produce significant damage, a span to thickness ratio of 32:1 was used for all three-point bend testing. Throughout the duration of the tests, the electrical impedance of the sample was determined using the standard four-probe method shown in Fig. 1d. Specifically, 3 mA of direct current (DC) was sent through the test specimen using the two silver paint rings at the opposite ends of the sample. The voltage across the two inside silver paint rings was then measured throughout the duration of the test using a NI 4431 DAQ, and the resistance of the sample was calculated during post-processing according to Ohm's law. Similar to the tensile tests, a high frequency microphone (PCB 426A05) was attached to the test frame close to the sample to confirm damage through acoustic emissions, and was read through a PCB 482A16 signal conditioner which was then connected to the NI 4431 DAQ. Due to the fact that the LIG coatings are located on the surface of only one side of each fiberglass prepreg layer, the samples are inherently asymmetric and the LIG surfaces are primarily in compression (LIG surfaces facing up) or tension (LIG surfaces facing down) as illustrated in Fig. 2a and Fig. 2b, respectively. For this reason, four three-point bend samples were tested in each configuration to establish differences in sensing potential during compression and tension.

3. Results and discussion

3.1. LIG characterization

The LIG surface on the Kapton® tape directly after printing was characterized using scanning electron microscopy (SEM), and the resulting images shown in Fig. 3a–c indicate that the LIG consists of a porous nanostructure which is comprised of interlaced graphene fibers. The nanostructure of the LIG can be controlled by varying the output

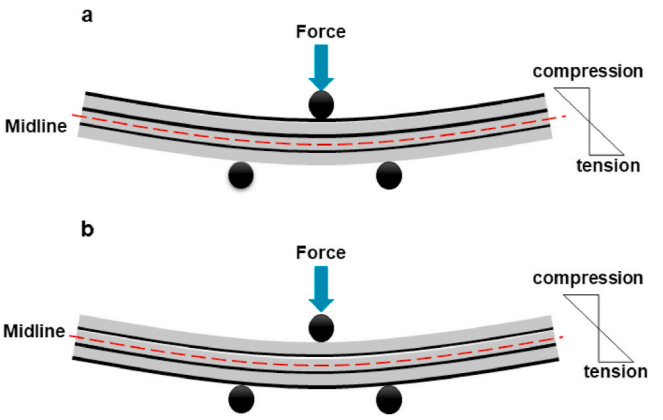

Fig. 2. Schematic of three-point bend configuration with LIG surfaces primarily under (a) compression and (b) tension.

power and pulsing density of the laser, however, the nanostructure seen in Fig. 3 was determined to provide the most effective transfer from the polyimide tape to the prepreg, thus resulting in the most advantageous conductivity for piezoresistive measurements. In detail, an output power of 14% and pulsing density (IUA) of 400 DPI was used to generate the LIG arrays prior to transfer printing. Additionally, to confirm the structure of the LIG was not altered during the transfer process from the polyimide tape to the fiberglass prepreg, additional SEM images were taken of the LIG coated prepreg surface following the transfer. As can be seen in Fig. 3d–e, the LIG nanostructure remains intact following the transfer, maintaining a similar surface morphology and alignment as was seen following the initial laser treatment. It should be noted that the fuzzy texture observed is drastically changed from the initial smooth surface of the as-received fiberglass prepreg. It is also clear from Fig. 3f–h that post-curing, the LIG is embedded within the matrix of the fiberglass prepreg following the transfer, thus reinforcing the matrix in a controlled manner prior to the layup of the composite. During the curing process, the matrix solidifies around the LIG thus fully integrating the LIG within the composite. The resulting resistivity values of the 3-ply samples range between 1.45 and 5.56 Ω·m for the angle-ply and unidirectional composites, both of which were 11–14 mm wide and 65–76 mm long.

3.2. Mechanical properties

DSC analysis was used to confirm that the addition of the LIG did not affect the cure of the sample. The results from both a neat fiberglass prepreg composite and a fiberglass prepreg composite with LIG are shown in Fig. 4a. From the results, both the neat fiberglass and fiberglass with LIG samples follow the same trend throughout the cure cycle, thus indicating that no significant change to the curing reaction of the composite due to the addition of the LIG is observed. Additionally, dynamic mechanical analysis was used to establish the relative changes in the viscoelastic properties of the composites containing LIG in comparison to those of the neat composite samples. The damping properties of fiberglass-reinforced composites play an important role during dynamic loading which is commonly experienced in aircraft and automobile applications among others [42]. The resulting storage modulus, loss modulus, and tan δ averaged between the samples tested are shown in Fig. 4b–d, respectively. The results shown in the figure clearly indicate an increase in damping is observed in the average tan δ at the peak temperature, while the storage modulus remains relatively constant between the sample sets. Thus, the addition of the LIG interlayer within the fiberglass composites clearly contributes significant damping to the material at the peak physical displacement experienced at the transition temperature, which is calculated to be a ~12% increase in tan δ, while the damping at low temperature is maintained. The increase at the

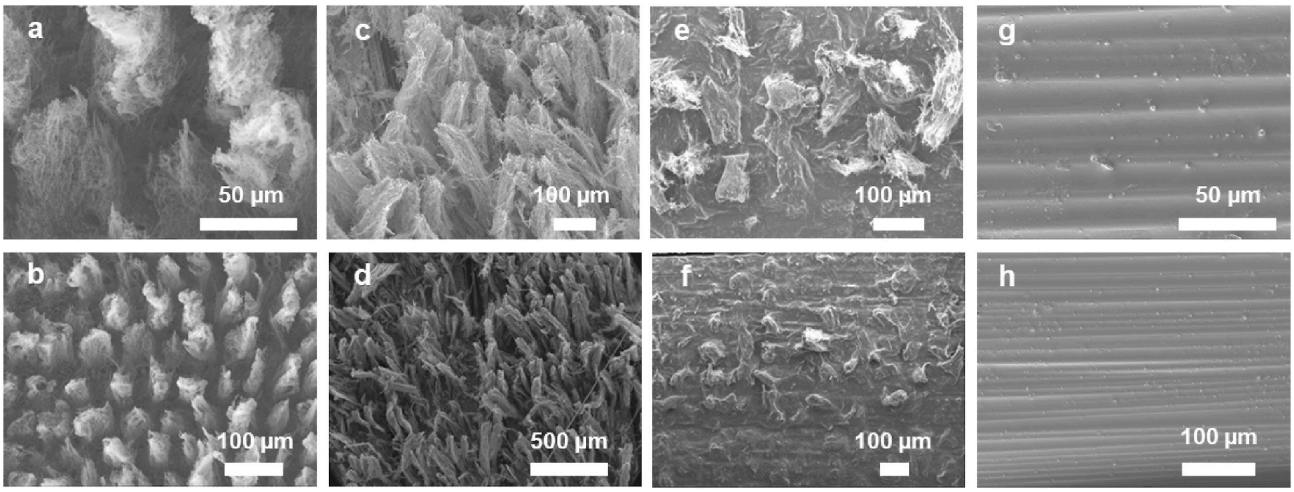

Fig. 3. (a–b) Scanning electron microscope (SEM) image of laser induced graphene (LIG) coating on polyimide tape. (c–d) SEM images of LIG coating on uncured fiberglass prepreg. (e–f) SEM images of LIG coating on cured fiberglass prepreg. (g–h) SEM images of cured neat fiberglass prepreg.

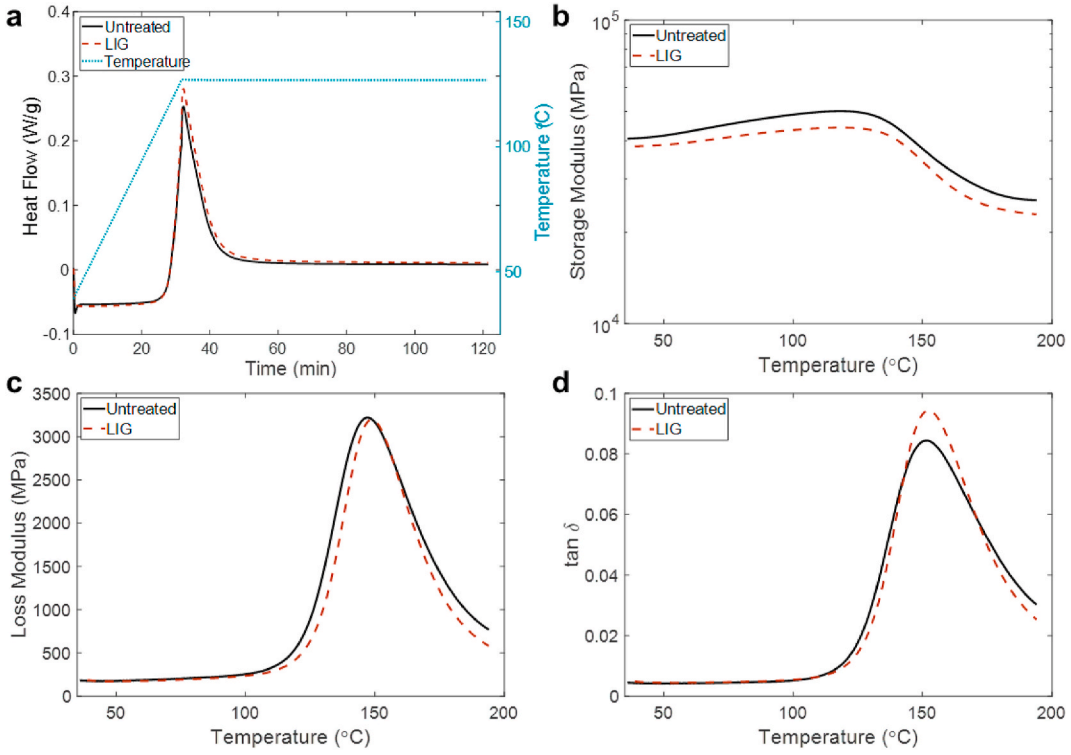

Fig. 4. (a) DSC results of heat flow versus time for a neat fiberglass sample and a fiberglass sample with LIG during curing cycle. Average (b) storage modulus, (c) loss modulus, and (e) tan δ of untreated fiberglass and fiberglass with LIG.

transition temperature is attributed to additional surface area between the fibers and the matrix due to the addition of the LIG in combination with the stick-slip phenomenon resulting from the interfacial friction between the fuzzy LIG and the matrix. Stick-slip behavior is commonly observed in composites containing CNTs due to the poor chemical bonding between the CNTs and the polymer matrix [43]. The carbon-based LIG is likely to exhibit similar behavior with the dominant mode of energy dissipation relying on friction at the interface between the LIG and the matrix. The mechanical energy from vibration of the sample is dissipated as heat through the interfacial friction resulting in the significantly improved damping. It should also be noted that since commercial prepreg was used for both sets of composites, the amount of epoxy matrix relative to the fiber content was held constant between the sample sets, so the fraction of epoxy does not play a role in the increase in damping. The LIG coating is therefore fully responsible for any observed increase in composite damping between the two sample sets. For reference, the mean value and standard deviation of the tan δ of both the untreated and LIG-treated samples at low temperature (50 °C) and the peak value is shown in Table 1.

Prior to the addition of the LIG interlayer, no treatment to the fibers was needed in this work, and since the LIG was introduced to the surface of existing commercial prepreg, the fibers were not altered or damaged during the transfer process. However, the LIG considerably modifies the structure of the interlaminar region of the composite, therefore, to confirm that the presence of the LIG does not weaken inter-ply strength and increase the risk of delamination, the short beam shear strength of

Table 1
Short beam shear strength, tan δ at low temperature, and peak tan δ values for untreated fiberglass composites and composites with LIG.

	Short Beam Shear Strength	tan δ @ 50 °C	Peak tan δ
Untreated	91.2 ± 1.34 MPa	0.0043 ± 0.00014	0.084 ± 0.008
LIG	90.4 ± 1.1 MPa	0.0044 ± 0.0002	0.094 ± 0.003

the fiberglass composite with the LIG surfaces was established using short beam shear testing. The short beam shear strength of the composites containing LIG was found to be approximately unchanged relative to that of the neat composites, with the LIG having a short beam shear strength of 90.4 ± 1.1 MPa and the untreated samples having short beam shear strength of 91.2 ± 1.34 MPa. In addition, an analysis of variance (ANOVA) test of the data reveals a p-value of 0.16, which is much higher than the typical cutoff value of 0.05, indicating that the null hypothesis is not rejected, and a statistically significant difference in the short beam shear strength is not present. Therefore, these results

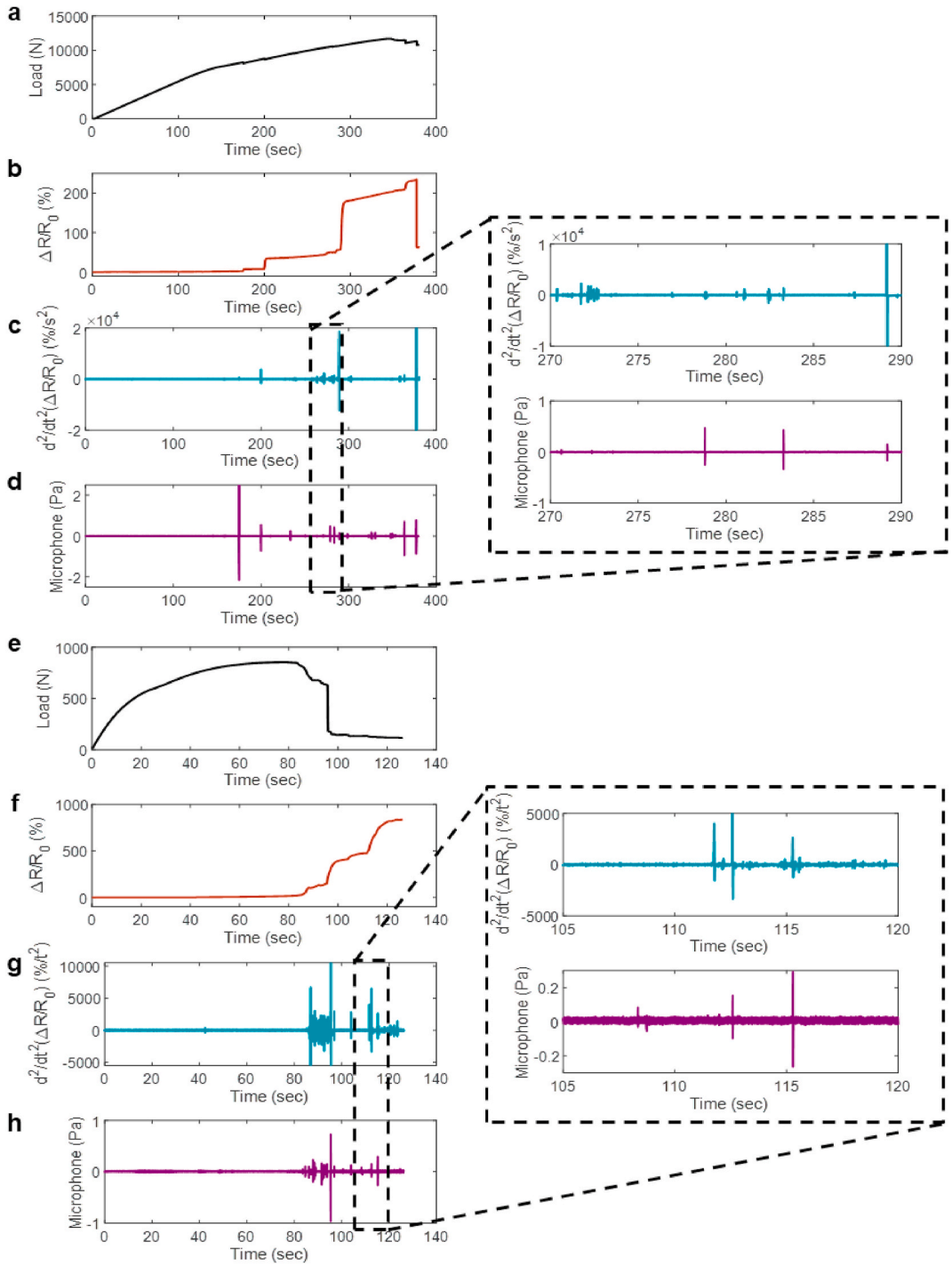

Fig. 5. (a) Applied load, (b) percent change in resistance, (c) second derivative of the percent change in resistance, and (d) microphone pressure reading for a unidirectional composite specimen with LIG under tensile loading. (e) Applied load, (f) percent change in resistance, (g) second derivative of the percent change in resistance, and (h) microphone pressure reading for a ±45° composite specimen with LIG under tensile loading.

confirm that the addition of the LIG to the surface of the fiberglass prepreg does not significantly weaken interlaminar adhesion between adjacent plies, thus avoiding an increase in the probability of delamination during application.

3.3. In-situ sensing during tensile testing

The fabricated samples were loaded in a tensile configuration to establish the capacity of the LIG coated fiberglass to sense tensile strain and failure. For greater visualization of sudden impedance changes, the second derivative of the impedance measurements, calculated numerically, was also considered. The resulting applied load, percent change in impedance, second derivative of the percent change in impedance, and microphone pressure of a representative unidirectional test specimen is shown in Fig. 5a–d respectively, and similar measurements for an angle ply test specimen are shown in Fig. 5e–h. For reference, the initial resistances of the angle ply test specimens were between approximately 300 and 1000 Ω while the initial resistances of the unidirectional specimens were between approximately 150 and 300 Ω. As a result of the piezoresistivity of the LIG interlayers in both samples, the electrical impedance and its second derivative show clear and distinct jumps, which are inversely proportional to sudden decreases in the applied load and correlate to detected acoustic emissions from the microphone. This is more clearly shown in the magnified sections of the second derivative and acoustic emission reading from the microphone. The combination of each of these measurements indicate significant damage to the specimens such as fiber failure or delamination as the samples near catastrophic failure. As each sample delaminates, the conductivity between LIG layers decreases as some of the carbon-carbon contacts are broken, resulting in an increase in measured impedance. Fiber failure also results in an irreversible increase in impedance as the LIG at each interface separates with the physical separation of the fiber and the surrounding matrix. The increase in impedance is proportional to the acoustic emissions indicating that the methods are comparable in their damage detection capabilities. However, as confirmed by the cyclic testing in Fig. 6 which is discussed further later, prior to significant damage as detected by the decreasing load and acoustic emissions from the microphone, the impedance of the sample increases approximately linearly due to the piezoresistive nature of the LIG interlayer. Specifically, as the sample is strained, the carbon-carbon contacts in the LIG coating separate resulting in the observed increase in impedance correlating to the increasing stress and strain. It should be noted that the sudden decrease in impedance observed from the unidirectional test specimen in Fig. 5e is an artifact from the electronic measurement as the wire disconnected from the sample at catastrophic failure.

To further investigate the in-situ strain sensing performance of the LIG coated fiberglass composites at low strains, cyclic testing with a maximum stress at approximately 50% of the ultimate strength was completed for the angle ply specimens. The resulting percent change in the electrical impedance of the test specimen in comparison to the percent change in strain as measured by a surface mounted strain gauge are shown in Fig. 6a. From the figure, the resistance of the sample follows the trend of the strain very closely, showing the ability of the LIG to act as an integrated strain sensor encapsulated within the composite. The gauge factor of the LIG was then calculated for each cycle (Fig. 6b) using the equation shown in Fig. 6b, where ΔR is the change in resistance, R_0 is the initial resistance of the sample at the beginning of each cycle, and ε is the strain measured using the commercial strain gauge. The average gauge factor for the fiberglass samples with integrated LIG was found to be 0.38 ± 0.05. It can be noted that this gauge factor is lower than the typical value of commercial strain gauges (~2) and alternative methods using embedded CNTs (1.6–4.14) [44,45], however, the integrated nature of the strain sensing mechanism removes the need for externally bonded sensors, and the methodology used here is more scalable than current nanofiller alternatives as discussed previously.

3.4. In-situ sensing during three-point bend testing

To determine the ability of the LIG interlayer to sense flexural loading, the samples were tested by means of three-point bend in two configurations: the LIG surfaces facing toward the top of the sample and the LIG surfaces facing toward the bottom of the sample. Due to the inherent asymmetry of the sample shown in Fig. 2, the LIG sensing layers experience dominant compression forces or tension forces if the LIG surfaces face upward or downward during testing, respectively. The results of the flexural bending tests for a representative sample in the compression and tension configurations can be seen in Fig. 7a–d and Fig. 7e–g, respectively. Both figures clearly show sudden and dramatic increases in electrical impedance with the occurrence of damage toward the end of the test as the sample approaches catastrophic failure as seen in both the impedance measurements as well as the second numerical derivative of the percent change in impedance. These increases in impedance also correlate to sudden drops in load and acoustic emissions detected using the high frequency microphone, thus confirming the occurrence of damage. This indicates that as sudden delamination or fiber fracture occur, the carbon-carbon contacts comprising the LIG surfaces are separated, thus increasing the impedance and resulting in a corresponding acoustic emission which is detected by the high frequency microphone. However, the percent increase in impedance correlated with damage was observed to be different between the samples in the compression configuration versus the samples in the tension configuration. Since more LIG surfaces experienced separation between the conductive carbon-carbon contacts with additional layers under tension, and the cumulative amount of separation was larger when the LIG layer was located at the point of maximum strain at the bottom of the sample. The total percent increase in impedance of the composite in the tension configuration was thus observed to be significantly higher than that under compression. In addition, the ability of the samples to track low levels of flexural strain was also different between

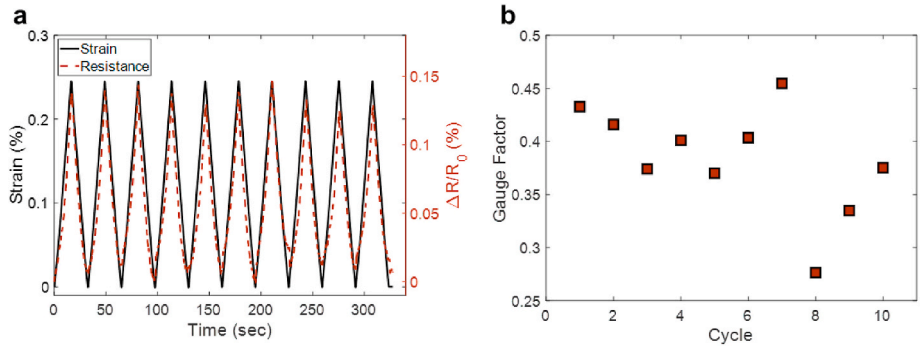

Fig. 6. (a) Percent strain measured using commercial strain gauge and percent increase in resistance from test specimen with LIG. (b) Gauge factor versus cycle.

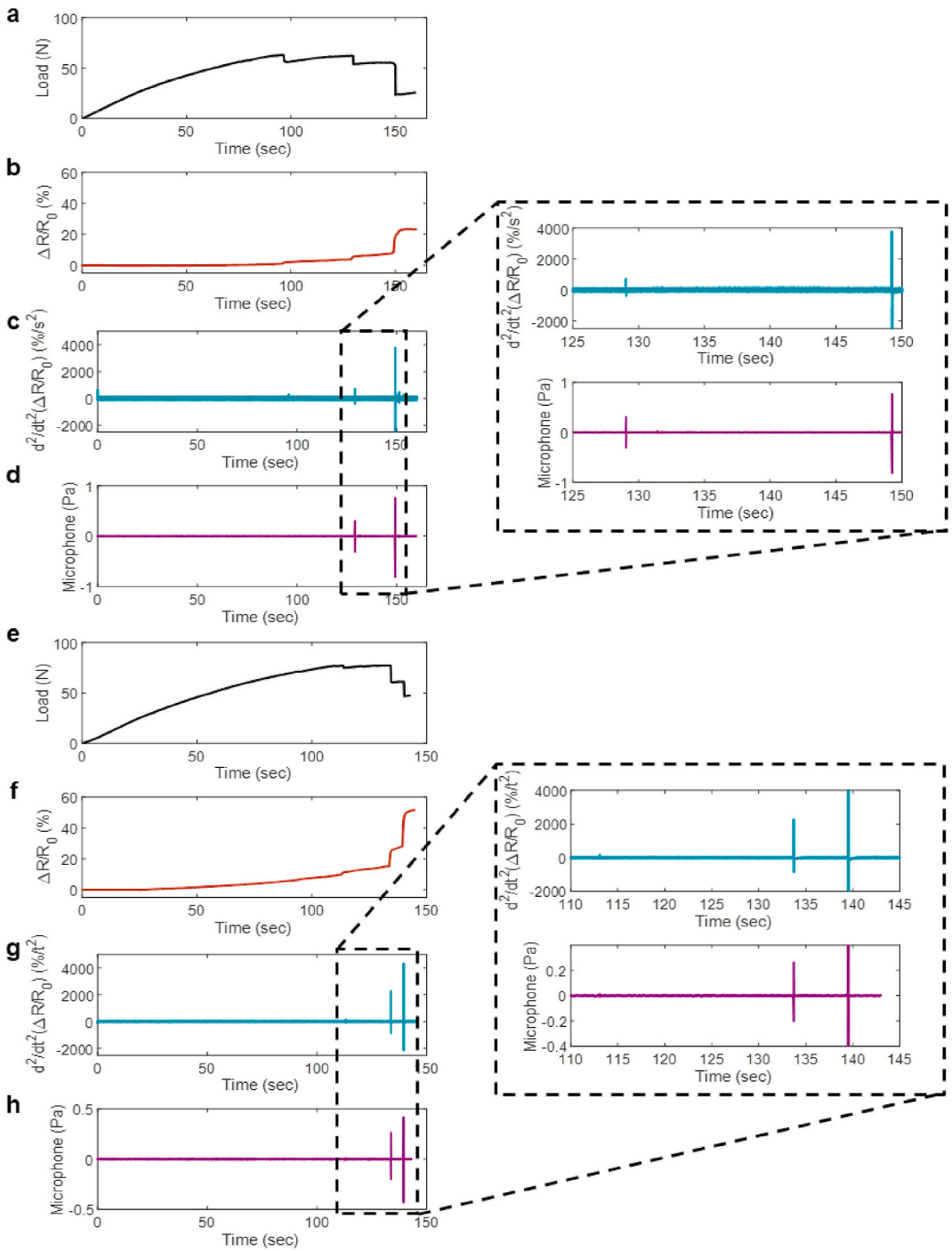

Fig. 7. (a) Load, (b) percent change in resistance, (c) second derivative of the percent change in resistance, and (d) microphone pressure for three-point bend specimen with LIG primarily under compression. (e) Load, (f) percent change in resistance, (g) second derivative of the percent change in resistance, and (h) microphone pressure for three-point bend specimen with LIG primarily under tension.

the samples under primary compression and the samples under primary tension. As LIG coated samples are compressed, a small amount of additional conductive carbon contacts are formed in each LIG interlayer, resulting in increased conductivity and a decrease in the measured impedance. In the case of a flexural sample, transverse compression and decreased impedance happens simultaneously to the separation of carbon contacts in the LIG interlayers under tension, resulting in cancellation between the two effects and a lower magnitude change in impedance compared to the sample experiencing primary tension in the LIG interlayers. Therefore, samples in both configurations are capable of detecting damage and sensing strain, however, the degree to which they are able to sense flexural strain is dependent on the orientation of the LIG interlayers.

4. Conclusion

This work establishes the use of a multifunctional LIG interlayer for in-situ monitoring of strain and damage in fiberglass-reinforced composites. The piezoresistive interlayer is coated directly onto commercial fiberglass prepreg using a cost-effective, simple, and scalable method, after which the health of the interlaminar region of the composite is confirmed to be maintained using short-beam shear testing. The

damping of the fiberglass composites with LIG was established using dynamic mechanical analysis which showed improved vibration energy dissipation at the transition temperature (~12% increase in tan δ) and maintained viscoelastic properties at temperatures closer to the nominal operating temperature. Furthermore, the piezoresistive sensing ability of the composites containing LIG was then established during flexural loading, tensile loading, and cyclic loading as the LIG proves capable of tracking both strain and detecting damage in situ via a standard four-point probe resistance measurement. The result of this work thus enables the integration of an in-situ sensing mechanism into a standard composite using simple methods, while also resulting in maintained mechanical properties of the host composite. Thus, any need for external sensors for the material is removed. Moreover, the techniques presented here are highly scalable and automatable relative to the current methods adopted to introduce piezoresistivity in fiberglass composites.

Declaration of competing interest

The authors declare that they have no known competing financial interests or personal relationships that could have appeared to influence the work reported in this paper.

CRediT authorship contribution statement

LoriAnne Groo: Conceptualization, Investigation, Writing - original draft. **Jalal Nasser:** Conceptualization, Investigation, Writing - review & editing. **Lisha Zhang:** Investigation, Writing - review & editing. **Kelsey Steinke:** Investigation, Writing - review & editing. **Daniel Inman:** Project administration, Methodology, Writing - review & editing. **Henry Sodano:** Conceptualization, Project administration, Methodology, Funding acquisition, Supervision, Writing - review & editing.

Acknowledgements

This work was supported by the National Science Foundation Graduate Research Fellowship Program under grant # DGE1256260 and a National Science Foundation grant # CMMI-1762369.

References

[1] T.P. Sathishkumar, S. Satheeshkumar, J. Naveen, Glass fiber-reinforced polymer composites – a review, J. Reinforc. Plast. Compos. 33 (13) (2014) 1258–1275.
[2] P.J. Schilling, B.R. Karedla, A.K. Tatiparthi, M.A. Verges, P.D. Herrington, X-ray computed microtomography of internal damage in fiber reinforced polymer matrix composites, Compos. Sci. Technol. 65 (14) (2005) 2071–2078.
[3] F. Awaja, M.-T. Nguyen, S. Zhang, B. Arhatari, The investigation of inner structural damage of UV and heat degraded polymer composites using X-ray micro CT, Compos. Appl. Sci. Manuf. 42 (4) (2011) 408–418.
[4] S. Barré, M. Benzeggagh, On the use of acoustic emission to investigate damage mechanisms in glass-fibre-reinforced polypropylene, Compos. Sci. Technol. 52 (3) (1994) 369–376.
[5] M.A. Hamstad, A review: acoustic emission, a tool for composite-materials studies, Exp. Mech. 26 (1) (1986) 7–13.
[6] T. Krause, S. Preihs, J. Ostermann, Acoustic emission damage detection for wind turbine rotor blades using airbore sound, in: Proceedings of 10th International Workshop on Structural Health Monitoring, IWSHM), 2015.
[7] G. Kister, B. Ralph, G.F. Fernando, Damage detection in glass fibre-reinforced plastic composites using self-sensing E-glass fibres, Smart Mater. Struct. 13 (5) (2004) 1166.
[8] K. Kuang, W. Cantwell, Use of conventional optical fibers and fiber Bragg gratings for damage detection in advanced composite structures: a review, Appl. Mech. Rev. 56 (5) (2003) 493–513.
[9] L. Böger, M.H. Wichmann, L.O. Meyer, K. Schulte, Load and health monitoring in glass fibre reinforced composites with an electrically conductive nanocomposite epoxy matrix, Compos. Sci. Technol. 68 (7–8) (2008) 1886–1894.
[10] S.l. Gao, R.C. Zhuang, J. Zhang, J.W. Liu, E. Mäder, Glass fibers with carbon nanotube networks as multifunctional sensors, Adv. Funct. Mater. 20 (12) (2010) 1885–1893.
[11] C. Baron, K. Schulte, Electric Resistance Measurement for in Situ Determination of Fiber Failure in Carbon Fiber Reinforced Laminates, 1988.
[12] K. Schulte, C. Baron, Load and failure analyses of CFRP laminates by means of electrical resistivity measurements, Compos. Sci. Technol. 36 (1) (1989) 63–76.
[13] X. Wang, X. Fu, D.D.L. Chung, Strain sensing using carbon fiber, J. Mater. Res. 14 (3) (2011) 790–802.
[14] J.C. Abry, S. Bochard, A. Chateauminois, M. Salvia, G. Giraud, In situ detection of damage in CFRP laminates by electrical resistance measurements, Compos. Sci. Technol. 59 (6) (1999) 925–935.
[15] S. Wang, D. Chung, Self-sensing of flexural strain and damage in carbon fiber polymer-matrix composite by electrical resistance measurement, Carbon 44 (13) (2006) 2739–2751.
[16] S. Wang, D.D.L. Chung, J.H. Chung, Impact damage of carbon fiber polymer–matrix composites, studied by electrical resistance measurement, Compos. Appl. Sci. Manuf. 36 (12) (2005) 1707–1715.
[17] J. Wen, Z. Xia, F. Choy, Damage detection of carbon fiber reinforced polymer composites via electrical resistance measurement, Compos. B Eng. 42 (1) (2011) 77–86.
[18] E.T. Thostenson, T.-W. Chou, Carbon nanotube networks: sensing of distributed strain and damage for life prediction and self healing, Adv. Mater. 18 (21) (2006) 2837–2841.
[19] H. Deng, L. Lin, M. Ji, S. Zhang, M. Yang, Q. Fu, Progress on the morphological control of conductive network in conductive polymer composites and the use as electroactive multifunctional materials, Prog. Polym. Sci. 39 (4) (2014) 627–655.
[20] H. Mahmood, L. Vanzetti, M. Bersani, A. Pegoretti, Mechanical properties and strain monitoring of glass-epoxy composites with graphene-coated fibers, Compos. Appl. Sci. Manuf. 107 (2018) 112–123.
[21] N. Muto, Y. Arai, S.G. Shin, H. Matsubara, H. Yanagida, M. Sugita, T. Nakatsuji, Hybrid composites with self-diagnosing function for preventing fatal fracture, Compos. Sci. Technol. 61 (6) (2001) 875–883.
[22] A. Godara, L. Gorbatikh, G. Kalinka, A. Warrier, O. Rochez, L. Mezzo, F. Luizi, A. W. van Vuure, S.V. Lomov, I. Verpoest, Interfacial shear strength of a glass fiber/epoxy bonding in composites modified with carbon nanotubes, Compos. Sci. Technol. 70 (9) (2010) 1346–1352.
[23] C.S. Grimmer, C.K.H. Dharan, High-cycle fatigue of hybrid carbon nanotube/glass fiber/polymer composites, J. Mater. Sci. 43 (13) (2008) 4487–4492.
[24] L. Gao, T.-W. Chou, E.T. Thostenson, Z. Zhang, M. Coulaud, In situ sensing of impact damage in epoxy/glass fiber composites using percolating carbon nanotube networks, Carbon 49 (10) (2011) 3382–3385.
[25] L. Gao, E.T. Thostenson, Z. Zhang, T.-W. Chou, Sensing of damage mechanisms in fiber-reinforced composites under cyclic loading using carbon nanotubes, Adv. Funct. Mater. 19 (1) (2009) 123–130.
[26] L. Gao, E.T. Thostenson, Z. Zhang, J.-H. Byun, T.-W. Chou, Damage monitoring in fiber-reinforced composites under fatigue loading using carbon nanotube networks, Phil. Mag. 90 (31–32) (2010) 4085–4099.
[27] M. Tehrani, A. Boroujeni, T. Hartman, T. Haugh, S. Case, M. Al-Haik, Mechanical characterization and impact damage assessment of a woven carbon fiber reinforced carbon nanotube–epoxy composite, Compos. Sci. Technol. 75 (2013) 42–48.
[28] F. Gojny, M. Wichmann, U. Köpke, B. Fiedler, K. Schulte, Carbon nanotube-reinforced epoxy-composites: enhanced stiffness and fracture toughness at low nanotube content, Compos. Sci. Technol. 64 (15) (2004) 2363–2371.
[29] N.D. Alexopoulos, C. Bartholome, P. Poulin, Z. Marioli-Riga, Structural health monitoring of glass fiber reinforced composites using embedded carbon nanotube (CNT) fibers, Compos. Sci. Technol. 70 (2) (2010) 260–271.
[30] J. Lin, Z. Peng, Y. Liu, F. Ruiz-Zepeda, R. Ye, E.L. Samuel, M.J. Yacaman, B. I. Yakobson, J.M. Tour, Laser-induced porous graphene films from commercial polymers, Nat. Commun. 5 (2014) 5714.
[31] Z. Peng, R. Ye, J.A. Mann, D. Zakhidov, Y. Li, P.R. Smalley, J. Lin, J.M. Tour, Flexible boron-doped laser-induced graphene microsupercapacitors, ACS Nano 9 (6) (2015) 5868–5875.
[32] L. Li, J. Zhang, Z. Peng, Y. Li, C. Gao, Y. Ji, R. Ye, N.D. Kim, Q. Zhong, Y. Yang, High-performance pseudocapacitive microsupercapacitors from laser-induced graphene, Adv. Mater. 28 (5) (2016) 838–845.
[33] L.-Q. Tao, H. Tian, Y. Liu, Z.-Y. Ju, Y. Pang, Y.-Q. Chen, D.-Y. Wang, X.-G. Tian, J.-C. Yan, N.-Q. Deng, An intelligent artificial throat with sound-sensing ability based on laser induced graphene, Nat. Commun. 8 (2017) 14579.
[34] R. Ye, D.K. James, J.M. Tour, Laser-induced graphene: from discovery to translation, Adv. Mater. 31 (1) (2019) 1803621.
[35] Y. Li, D.X. Luong, J. Zhang, Y.R. Tarkunde, C. Kittrell, F. Sargunaraj, Y. Ji, C. J. Arnusch, J.M. Tour, Laser-induced graphene in controlled atmospheres: from superhydrophilic to superhydrophobic surfaces, Adv. Mater. 29 (27) (2017) 1700496.
[36] D.X. Luong, K. Yang, J. Yoon, S.P. Singh, T. Wang, C.J. Arnusch, et al., Laser-induced graphene composites as multifunctional surfaces, ACS Nano 13 (2) (2019) 2579–2586.
[37] L.X. Duy, Z. Peng, Y. Li, J. Zhang, Y. Ji, J.M. Tour, Laser-induced graphene fibers, Carbon 126 (2018) 472–479.
[38] J. Nasser, J. Lin, L. Zhang, H.A. Sodano, Laser induced graphene printing of spatially controlled super-hydrophobic/hydrophilic surfaces, Carbon 162 (2020) 570–578.
[39] R. Rahimi, M. Ochoa, W. Yu, B. Ziaie, Highly stretchable and sensitive unidirectional strain sensor via laser carbonization, ACS Appl. Mater. Interfaces 7 (8) (2015) 4463–4470.
[40] Y. Wang, Y. Wang, P. Zhang, F. Liu, S. Luo, Laser-induced freestanding graphene papers: a new route of scalable fabrication with tunable morphologies and properties for multifunctional devices and structures, Small 14 (36) (2018) 1802350.
[41] W. Cui, M.R. Wisnom, M. Jones, Effect of specimen size on interlaminar shear strength of unidirectional carbon fibre-epoxy, Compos. Eng. 4 (3) (1994) 299–307.
[42] R. Chandra, S.P. Singh, K. Gupta, Damping studies in fiber-reinforced composites – a review, Compos. Struct. 46 (1) (1999) 41–51.

[43] X. Zhou, E. Shin, K.W. Wang, C.E. Bakis, Interfacial damping characteristics of carbon nanotube-based composites, Compos. Sci. Technol. 64 (15) (2004) 2425–2437.

[44] J. Sebastian, N. Schehl, M. Bouchard, M. Boehle, L. Li, A. Lagounov, K. Lafdi, Health monitoring of structural composites with embedded carbon nanotube coated glass fiber sensors, Carbon 66 (2014) 191–200.

[45] G.J. Gallo, E.T. Thostenson, Electrical characterization and modeling of carbon nanotube and carbon fiber self-sensing composites for enhanced sensing of microcracks, Mater. Today Commun. 3 (2015) 17–26.